Structure optimization of task-specific ionic liquids targeting low-carbon-emission ethylbenzene production

Lei, Yang; Yu, Zhaoyang; Wei, Zhiqiang; Liu, Xinyan; Yu, Haoshui; Liang, Xiaodong; Kontogeorgis, Georgios M.; Chen, Yuqiu

Published in:
Separation and Purification Technology

DOI (link to publication from Publisher):
10.1016/j.seppur.2022.122827

Publication date:
2023

Document Version
Publisher's PDF, also known as Version of record

Separation and Purification Technology 308 (2023) 122827

Contents lists available at ScienceDirect

Separation and Purification Technology

journal homepage: www.elsevier.com/locate/seppur

Structure optimization of task-specific ionic liquids targeting low-carbon-emission ethylbenzene production

Yang Lei [a], Zhaoyang Yu [a], Zhiqiang Wei [b], Xinyan Liu [a,*], Haoshui Yu [c], Xiaodong Liang [d], Georgios M. Kontogeorgis [d], Yuqiu Chen [d,*]

[a] School of Chemistry and Chemical Engineering, Hubei Key Laboratory of Coal Conversion and New Carbon Materials, Wuhan University of Science and Technology, Wuhan 430081, Hubei, China
[b] Sinopec Engineering Incorporation, Beijing 100101, China
[c] Department of Chemistry and Bioscience, Aalborg University, Niels Bohrs Vej 8A, Esbjerg 6700, Denmark
[d] Department of Chemical and Biochemical Engineering, Technical University of Denmark, Lyngby 2800, Denmark

ARTICLE INFO

Keywords:
Ethylbenzene production
Ionic liquid
CAILD
Extractive distillation
Carbon emission

ABSTRACT

The production of ethylbenzene from dry gas is a representative of an energy-intensive process in oil refineries, and the distillation process accounts for the major energy consumption and carbon emissions. Due to the increasing energy and environmental challenges, there is a strong demand for new technologies or intensified process designs that enable us to have energy-efficient and sustainable process operations. In this work, an ionic liquid (IL)-based energy-efficient extractive distillation (ED) process with low carbon emission is proposed for the distillation process of ethylbenzene production from dry gas. First, the structure of task-specific ILs is optimized through the computer-aided IL design (CAILD) method with a novel design objective. An ammonium-based IL ethylammonium trifluoromethanesulfonate ($[C_2H_8N][TfO]$), that has the best objective performance, is identified by solving a mixed-integer nonlinear programming (MINLP) problem. The energy, environmental (carbon emission), and economic performance of this $[C_2H_8N][TfO]$-based ED process in the ethylbenzene production is then thoroughly evaluated on the basis of optimized process operations in Aspen Plus. For demonstration purposes, a case study for the separation process of an industrial-scale ethylbenzene production in a Chinese refining industry is performed. When compared to the conventional process that is currently used in the petrochemical industry, our proposed $[C_2H_8N][TfO]$-based ED separation process has 40 % energy (hot utility) savings and a 11 % cost reduction. Notably, the IL-based ED separation process has 40 % lower carbon emissions versus the conventional process, indicating its great potential for sustainable operation in the production of ethylbenzene from dry gas.

1. Introduction

Ethylbenzene (EB) is a significant high-output petrochemical in the petrochemical community. More than 90 % of EB is used to produce styrene, one of the most important intermediates that is widely used in the production of fibers, rubbers, and resins [1]. In industry, most EB is produced on a large scale from ethylene and benzene in an acid-catalyzed chemical conversion. Currently, the pure-ethylene and the dilute-ethylene process are the two main processes applied to the production of EB. The further development and industrial application of the former process is largely limited due to the strict purity requirement of ethylene as well as the fast increase of olefin demand accompanied with the increasing shortage of oil. On the other hand, fluid catalytic cracking tail gas, also known as dry gas, which contains 10 % – 30 % ethylene, can also be used to produce EB after serval appropriate processes. Producing EB from dilute ethylene can not only make the efficient utilization of depletable resources, but also reduce production costs and carbon emissions. The dilute-ethylene process has essential improvements in the chemical industry over the past three decades.

The production of EB from dry gas generally contains three steps: dry gas refining, EB reaction, and EB distillation. This production is an energy-intensive and high carbon emission process, and the EB distillation part accounts for the major energy consumption and carbon emissions [2]. Therefore, any new methods or technologies of process intensification that allow us to have energy-efficient and sustainable EB

* Corresponding authors.
E-mail addresses: liuxinyan@wust.edu.cn (X. Liu), yuqch@kt.dtu.dk (Y. Chen).

https://doi.org/10.1016/j.seppur.2022.122827
Received 7 October 2022; Received in revised form 11 November 2022; Accepted 29 November 2022
Available online 5 December 2022

List of Abbreviations

ACC	Annualized capital cost
CAILD	Computer-aided ionic liquid design
CAMD	Computer-aided molecular design
DC	Distillation column
DC1	benzene column
DC2	ethylbenzene column
DC3	diethyl benzene column
EB	Ethylbenzene
ED	Extractive distillation
EDC	Extractive distillation column
EDC1	Extractive distillation benzene column
EDC2	Extractive distillation ethylbenzene column
EDC3	Extractive distillation diethyl benzene column
SRC	Solvent recovery column
GC	Group contribution
HP	High pressure
IL	Ionic liquid
MINLP	Mixed-integer nonlinear programming
N_{ST}	Number of equilibrium stages
OPEX	Operating cost
RR	Reflux ratio
SEC	Specific energy consumption
SRC	Solvent recovery column
S/F	Mass ratio of solvent
TAC	Total annual cost
TEC	Total energy consumption
a_j	anion group described by binary variables
c_i	cation group described by binary variables
g_l	side chain described by binary variables
M_{IL}	molecular weight of ILs
n_{kl}	number of substituent groups on the side chain
P_B^S	saturated vapor pressure of benzene
P_{EB}^S	saturated vapor pressure of ethylbenzene
T_m	melting point
T_p	temperature of every processing unit
v_i	the group valence of cations
v_{kl}	the group valence of substituents
$\gamma_{B,IL}^{\infty}$	dilution activity coefficient of benzene
$\gamma_{DB,IL}^{\infty}$	infinite dilution activity coefficient of diethyl benzene in the IL solvent
$\gamma_{EB,IL}^{\infty}$	infinite dilution activity coefficient of ethylbenzene
$\gamma_{HK,IL}^{\infty}$	infinite dilution activity coefficient of the heavy key component in the IL solvent
$\gamma_{LK,IL}^{\infty}$	infinite dilution activity coefficient of the light key component in the IL solvent
$\vartheta_{mass}^{\alpha}$	mass-based design target

production are critical for mitigating the issue of energy shortage and global warming caused by carbon emissions. To date, different design and optimization approaches have been recommended to improve the energy performance, economic and environmental performance which have been investigated of EB production from dry gas. For the EB distillation process, the studied alternative methods include extractive distillation [3], azeotropic distillation [4], reactive distillation [5], *etc*. Similar to many other energy-intensive and different separations, IL (ionic liquid)-based distillation processes have also received more attention in the separation of benzene homologues as ILs generally have negligible vapor pressure, high thermal stability, and they also have good selectivity for a wide range of chemicals [6–8].

The IL-based extractive distillation has been widely studied in many separation processes [9], such as [EMIM] [TCM] is employed in the aromatic/aliphatic separation [10,11]. Table 1 summarizes the published works using ILs for the separation of benzene homologues. So far, most reported ILs are imidazolium and pyridinium solvents, and their applications are limited to separate binary mixtures of benzene homologues. However, in industry, the EB separation process usually consists of 3–4 distillation columns because the stream from the EB reaction process is a multicomponent mixture. Therefore, ILs that can promote the separation of benzene homologues in all distillation columns are essential for the implementation of IL-based EB separation technology in the industry. As we know, the number of potential IL candidates is so large, and it would be extremely challenging to find suitable ILs that can meet the separation requirements in all distillation columns. In this regard, the computer-aided molecular design (CAMD) approach is thoroughly based on predictive property formulas and optimization algorithms may have the potential to provide solutions for this challenging problem. Unlike the trial-and-error method which generally is time-consuming and expensive, the computer-aided design method is more systematic and cost-effective.

As reported, the computer-aided ionic liquid design (CAILD) method has been efficiently employed to screen high-performance ILs for different purposes, including gas separation [12,13], bioproduct recovery [14,15], separation of near azeotropic system, and azeotropic mixtures [16–19], *etc*. The quality of the solutions from CAILD-based design problems mainly depends on the reliability of the used property models and optimization algorithms. By far, thermodynamic models such as UNIFAC [12–15,19,20], NRTL [21–33]、COSMO-RS [34–41], and UNIQUAC [25,28] have been employed to study the thermodynamic behavior of IL-organic chemical systems. Among these studied thermodynamic models, UNIFAC being a group contribution (GC)-based model, is the most widely applied one in CAILD. This is because the UNIFAC model not only can be easily integrated into CAILD models, but also usually provides good quantitative predictions. Meanwhile, GC-based models developed in our previous work can be used to predict the physical properties of ILs. Furthermore, optimization solvers such as LINGOGLOBAL and CPLEX in the general algebraic modeling system (GAMS) have been proven also to solve CAILD-based optimization models [42].

The research motivation of this work is to focus on the high energy consumption and high carbon emission of EB distillation units in practical applications. A novel IL-based ED process is firstly proposed to achieve energy-saving and low-carbon emission operation of the EB distillation process in the EB production from dry gas. In this process, the IL that can satisfy the separation requirements in all distillation columns is determined by solving a complex CAILD-based optimization model. The energy, environmental (carbon emission), and economic performance of this IL-based ED process are thoroughly evaluated following a rigorous simulation model in Aspen Plus. The application of this IL-based separation process is demonstrated through a case study at the level of a Chinese oil refining industry.

2. CAILDxxx

2.1. Mixed integer nonlinear programming (MINLP) model

Like many other decision-making optimization problems in process industries, the CAILD-based optimization problem also leads to a MINLP model combining discrete variables, continuous variables, and nonlinear equations in the objective equations and/or the constraint conditions. Table 2 summarizes the formulated MINLP model for the CAILD-based optimization problem targeting the EB distillation process.

Table 1
Reported ILs for separating benzene homologues.

Separation system	IL	Full name of IL	Refs
Hexane/benzene	[C_2MIM][NTf_2]	1-ethyl-3-methylimidazolium bis (trifluoromethylsulfonyl)imide	[43]
	[C_4MIM][NTf_2]	1-butyl-3-methylimidazolium bis (trifluoromethylsulfonyl)imide	
	[C_8MIM][NTf_2]	1-octyl-3-methylimidazolium bis (trifluoromethylsulfonyl)imide	
Benzene/*n*-octane /*n*-decane	[BMPYR][NTf_2]	1-butyl-1-methylpyrrolidinium bis(trifluoromethylsulfonyl) imide	[44]
Cyclohexane /benzene	[4BMPY][TCM]	1-butyl-4-methylpyridinium tricyanomethanide	[26]
Methylcyclohexane /benzene	[EPY][ESO_4]	1-ethylpyridinium ethylsulfate	[45]
Heptane/p-xylene	[BMIM][NO_3]	1-butyl-3-methylimidazolium nitrate	[46]
Octane/p-xylene	[OMIM][NO_3]	1-methyl-3-octylimidazolium nitrate	[46]
Benzene/ acetonitrile	[EMIM][BF_4]	1-ethyl-3-methylimidazolium tetrafluoroborate	[47]
n-hexane /benzene	[EMIM][NTf_2]	1-ethyl-3-methylimidazolium bis (trifluoromethylsulfonyl)imide	[48]
	[EMIM][$EtSO_4$]	1-ethyl-3-methylimidazolium ethylsulfate	
n-heptane/toluene	[EMIM][SCN]	1-ethyl-3-methylimidazolium thiocyanate	[49–51]
	[BMIM][SCN]	1-butyl-3-methylimidazolium thiocyanate-	
	[EMIM][DCA]	1-ethyl-3-methylimidazolium dicyanamide	
	[BMIM][DCA]	1-butyl-3-methylimidazolium dicyanamide	
	[EMIM][TCM]	1-ethyl-3-methylimidazolium tricyanomethanide	
	[BMIM][TCM])	1-butyl-3-me-thylimidazolium tricyanomethanide	
	[4BMPY][TCM]	1-butyl-4-me-thylpyridinium tricyanomethanide	
	[4EMPY][Tf2N]	1-ethyl-4-me-thylpyridinium bis (trifluoromethylsulfonyl)imid	[49,51]
	[4BMPY][Tf2N]	1-butyl-4-methylpyridinium bis (trifluoromethylsulfonyl)imid	
Toluene/*n*-heptane	[C_2C_1IM][TCM]	1-ethyl-3-methylimidazolium tricyanomethanide	[52]
	[4-C_4C_1PY][TCM]	1-butyl-4-methylpyridinium tricyanomethanide	
n-hexane + benzene	[C_2C_1IM][TCM]	1-ethyl-3-methylimidazolium tricyanomethanide	[53]
n-octane + p-xylene	[4-C_4C_1PY][TCM]	1-butyl-4-methylpyridinium tricyanomethanide	
n-octane + benzene	[C_2C_1IM][TCM]	1-ethyl-3-methylimidazolium tricyanomethanide	[54]
	[4-C_4C_1PY][TCM]	1-butyl-4-methylpyridinium tricyanomethanide	
n-heptane + benzene	[C_2C_1IM][TCM]	1-ethyl-3-methylimidazolium tricyanomethanide	
	[4-C_4C_1PY][TCM]	1-butyl-4-methylpyridinium tricyanomethanide	
n-octane + toluene	[C_2C_1IM][TCM]	1-ethyl-3-methylimidazolium tricyanomethanide	
	[4-C_4C_1PY][TCM]	1-butyl-4-methylpyridinium tricyanomethanide	

The IL structure is optimized by maximizing the mass-based design target (Eq. 1) that evaluates the separation performance of the IL. In this MINLP model, different IL functional groups (i.e. cations, anions, substituents) are totally combined subject to several molecular structural constraints (Eqs. 2–8), physical properties constraints (Eqs. 9 and 10), and thermodynamic property constraints (Eqs. 11 and 12).

In Eqs.2–8,*C*, *A* and*S*, respectively, denote the sets of cation groups, anion groups, and substituent groups. The occurrence of the cation group*i*, anion group*j*, and side chain *l* are described by binary variables ofc_i, a_i andg_l, respectively. The number of substituent group *k* on the side chain *l* is represented by integer variables ofn_{kl}, while the group valence of cations and substituents are expressed by integer variables of v_i andv_{kl}, respectively. n_S^L and n_S^U are the minimum and the maximum number of substituent group *k* in the whole IL molecule, while n_{SL}^L and n_{SL}^U are the are the minimum and the maximum number of substituent group *k* on the side*l*, respectively. The feasibility of the generated IL candidates is described by Eqs.2–6, wherein Eqs.2 and 3 are used to ensure there is only one cation and anion in each IL molecule, and Eq.4 is utilized to describe the octet rule that ensures the consistency between the number of side chains *N* and the free valence of the cation. Meanwhile, Eqs.5 and 6 are introduced to ensure that any two adjacent groups are not linked by more than one covalent bond. On the other hand, Eqs.7 and 8 are used to ensure the complexity of the generated IL candidates. Table 3 gives all the IL functional groups used in the CAILD-based optimization problem for the EB distillation process.

Table 2
MINLP model formulation for the CAILD-based optimization problem targeting EB distillation process.

Objective function (maximization)	$\vartheta_{mass}^{\alpha} = \frac{\gamma_{B,IL}^{\infty} P_B^S}{\gamma_{EB,IL}^{\infty} P_{EB}^S M_{IL}}$	(1)
Molecular structural constraints [38]	$\sum_{i\in C} c_i = 1$	(2)
	$\sum_{j\in A} a_i = 1$	(3)
	$\sum_{l=1}^{N} g_i - \sum_{i\in C} c_i v_i = 0$	(4)
	$\sum_{i\in C} c_i(2-v_i) + \sum_{l=1}^{N}\sum_{k\in S} g_i n_{kl}(2-v_{kl}) = 2$	(5)
	$\sum_{k\in S} g_i n_{kl}(2-v_{kl}) = 1$	(6)
	$n_S^L \leqslant \sum_{l=1}^{N}\sum_{k\in S} g_i n_{kl} \leqslant n_S^U$	(7)
	$n_{SL}^L \leqslant \sum_{k\in S} g_i n_{kl} \leqslant n_{SL}^U$	(8)
Physical property constraints	$T_m < T_p - 5(K)$	(9)
	$\eta < 0.1(Pa{\cdot}s)$	(10)
Thermodynamic property constraints	$\frac{\gamma_{LK,IL}^{\infty}}{\gamma_{HK,IL}^{\infty}} > 1$	(11)
	$\frac{1}{\gamma_{DB,IL}^{\infty}} < 100$	(12)

Table 3
IL functional groups used in the CAILD-based MINIP model for the EB distillation process.

Types	Groups		Groups
Substituents	CH_3	Anions	$[Tf_2N]^-$
	CH_2		$[BF_4]^-$
Cation skeletons	$[IM]^+$		$[PF_6]^-$
	$[MIM]^+$		$[CF_3COO]^-$
	$[Py]^+$		$[CF_3SO_3]^-$
	$[Mpy]^+$		$[MeSO_4]^-$
	$[CH_3N]^+$		$[EtSO_4]^-$
	$[C_2H_5N]^+$		$[MDEG]^-$
	$[C_3H_7N]^+$		$[Cl]^-$
	$[C_4H_9N]^+$		$[SCN]^-$

To avoid solvent solidification in practical operations, the melting point (T_m) of the IL solvent must be at least 5 K lower than the temperature of every processing unit, as expressed by Eq. 9. In the EB distillation process, the referenced temperature (350 K) is taken from the top of the benzene distillation column. As known, viscosity denotes opposition to flow, and therefore we use Eq. 10 to ensure that all the generated IL candidates have viscosity lower than 0.1 Pa·s (T = 298.15 K). These two physical properties of ILs can be, respectively, predicted from GC-based models [55,56].

Besides specifying appropriate design constraints, selecting a reasonable design objective is also critical to find high-performance ILs when using the CAILD method. In the distillation process, relative volatility (α) indicates the ease or difficulty to separate the volatile components from the less volatile components in a mixture. As a result, the ability to increase the relative volatility of different components in a mixture is a significant target to estimate the separation performance of

Table 4
Model summary of CAILD-based MINLP problem.

Continuous variables	Integer variables	Binary variables	Equations	Constraints	Iterations	Best solution time (s)
338	137	42	373	373	17,797	7

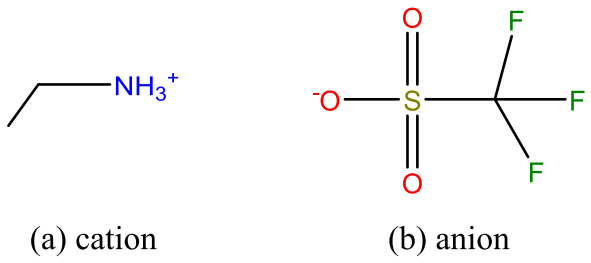

Fig. 1. Molecular structure of [C_2H_8N][TfO].

an IL. In industry, the cost of IL solvents is generally depended on their mass consumption, and it would be easier for us to find ILs with good economic performance if the molecular weight of ILs (M_{IL}) is considered in the design objective. For this reason, a mass-based design target ($\vartheta^{\alpha}_{mass}$), as formulated in Eq. 1, is employed as the objective function of the MINLP problem. In Eq. 1, P^{S}_{B} and P^{S}_{EB} denote the saturated vapor pressure of benzene and ethylbenzene, while $\gamma^{\infty}_{B,IL}$ and $\gamma^{\infty}_{EB,IL}$ describe the infinite dilution activity coefficient of benzene and ethylbenzene in the IL solvent, respectively. $\vartheta^{\alpha}_{mass}$ evaluates the mass-based separation performance of IL in the first distillation column (DC), which accounts for the most energy consumption of the whole EB distillation process (see Section 4). In addition, Eq. 11 is used to ensure that the IL solvent has a positive effect on the septation of the light key component and the heavy key component in all distillations, while Eq. 12 is utilized to control the difficulty of solvent recovery at a reasonable level. For the studied EB distillation process in this work (see Fig. 2), benzene is the light key component and EB is the heavy key component in EDC1; EB is the light key component and isopropybenzene is the heavy key component in EDC2; isopropybenzene is the light key component and diethylbenzene is the heavy key component in EDC3. $\gamma^{\infty}_{LK,IL}$ and$\gamma^{\infty}_{HK,IL}$, respectively, denote the infinite dilution activity coefficient of the light key component and the heavy key component in the IL solvent, while $\gamma^{\infty}_{DB,IL}$ describes the infinite dilution activity coefficient of diethylbenzene (the heaviest key component) in the IL solvent.

2.2. MINLP solution

The structure of the task-specific ILs is optimized by maximizing $\vartheta^{\alpha}_{mass}$ of the formulated MINLP problem in the GAMS, where LINDOGLOBAL is selected as the solver. The model statistics of the GAMS solution for this CAILD-based MINLP problem is summarized in Table 4. In this study, ethylammonium trifluoromethanesulfonate [C_2H_8N][TfO], which has a melting point of 336.4 K and a viscosity of 0.062 Pa·s (at 298.15 K), is defined as the best IL for the studied EB distillation process. The structure of this ammonium-based IL is given in Fig. 1. From the functional group level, the excellent separation performance of [C_2H_8N][TfO] can be demonstrated by the positive and strong interactions between its functional groups and the alkane/aromatic carbon-alkane groups in the EB molecule. Currently, experimental information of [C_2H_8N][TfO] is not available in the literature, but even combining the model uncertainty (±3.58 %), the maximum calculated viscosity of [C_2H_8N][TfO] (0.064 Pa.s) can still meet the design constraint of viscosity. On the other hand, the calculated melting point of [C_2H_8N][TfO] is between 314.2 K and 360.2 K after considering the model uncertainty (±7.07 %). Although the maximum calculated melting point is a little higher than the upper value in the design constraint, the actual melting point of [C_2H_8N][TfO] is probably close to 314.2 K as the reported melting point of another ammonium-based IL diethylmethylammonium trifluoromethanesulfonate ([$C_6H_{14}N$][TfO]) is only 268.1 K.

3. Process design

The [C_2H_8N][TfO]-based EB distillation process will be rigorously simulated and optimized in Aspen Plus V9. It's worth noting that two issues need to be addressed: (1) ILs are still not included in the component database of Aspen Plus. In this work, [C_2H_8N][TfO] will be defined as a pseudo component, and Table 5 gives all the information that required for pseudo-component definition in Aspen Plus. (2) Thermodynamic models that can describe systems containing ILs are not available in Aspen Plus. In this study, the UNIFAC-IL model [42] is used as it has been extended to the IL-organic chemical systems containing functional groups decomposed from [C_2H_8N][TfO]. And the good predictivity (AARD < 10 %) has been confirmed in previous work [57,58].

In addition to the simulation and optimization of the IL-based ED process, the conventional EB distillation process will also be simulated and optimized, and then the two processes will be systematically compared. The conventional EB distillation process contains three distillation columns, i.e., benzene column, ethylbenzene column, and diethyl benzene column (see Fig. 2a). The crude fractionator bottom oil (crude feed 1, see Table 6) and reverse alkylation products (crude feed 2, see Table 6) from the upstream are fed from the middle of the benzene column (DC1). 99.4 % of benzene is distilled from the top of the DC1. The substances at the bottom of the DC1 enter the ethylbenzene column (DC2), and 96.2 % of ethylbenzene is obtained at the top of the ethylbenzene column (DC2). The substances at the bottom of the DC2 enter the diethyl benzene column (DC3), and 25 kg/h of propyl benzene is distilled from the top of the DC3. The mass flow of propyl benzene in the material at the bottom of the DC3 is controlled to be less than 2 kg/h, and the purity of diethyl benzene at the bottom of the DC3 is 99.3 %. Different from the conventional EB separation process, the IL-based EB distillation process requires a solvent recovery column (SRC) to regenerate IL for its recycling, as shown in Fig. 2 (b). Fresh IL (S3) as extractant enters the extractive distillation benzene column (EDC1) from the upper part of the extractive distillation column, and benzene (S4) with greater than 99.4 wt% is obtained in EDC1. The mixture of IL and other benzene homologues enters the extractive distillation ethylbenzene column (EDC2), and 96.2 % ethylbenzene is obtained at the top of the EDC2. IL and the remaining benzene homologues at the bottom of the EDC2 enter the extractive distillation diethyl benzene column (EDC3), and propyl benzene is distilled from the top of the EDC3.

Table 5
Required information for pseudo-component definition of [C_2H_8N][TfO] in process simulation.

Solvents	MW (g/mol)	P_c [48] (bar)	T_c [48] (K)	V_c [48] (cm^3/mol)	API gravity	T_{nb} (K)	η (Pa s, 298.15 K)	ω
[C_2H_8N][TfO]	195.14	14.86	835.9	588.95	−30.73	645.62	0.062	0.69

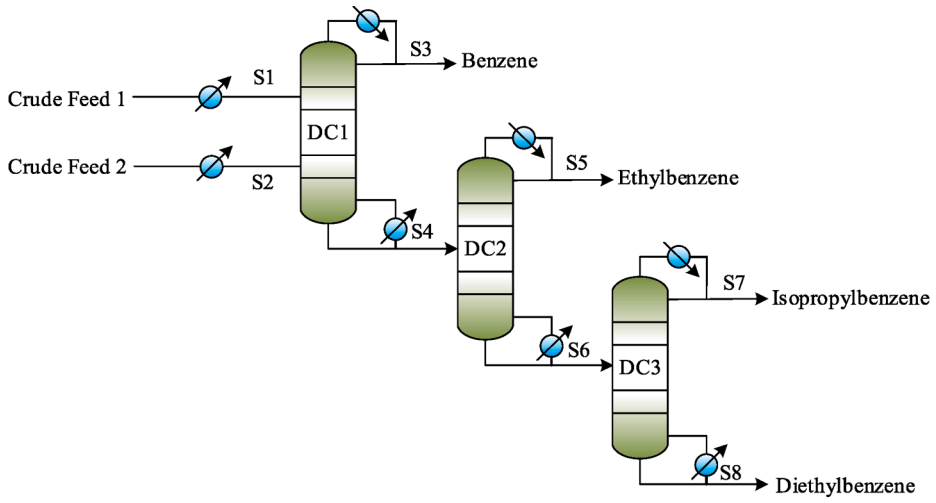

(a) Conventional EB distillation process

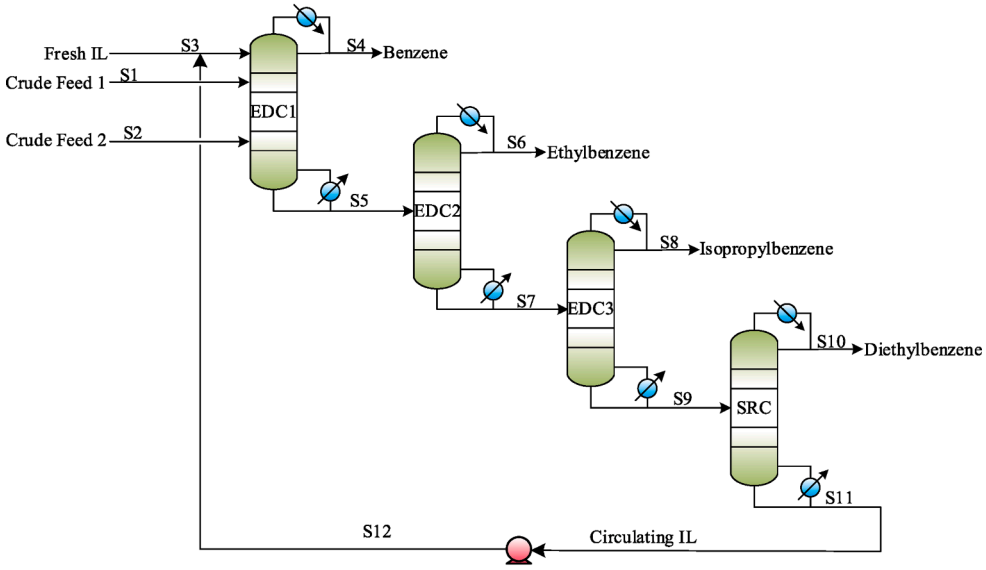

(b) The IL-based EB distillation process

Fig. 2. Flow diagram of EB distillation process.

Finally, IL and the rest of the benzene homologues enter SRC, where 99.3 % diethylbenzene is obtained at the top of the SRC and 99.9 % circulating IL is directly recycled to EDC1 through a pump.

The rigorous process simulations of an industrial-scale EB distillation process are performed, followed by an in-depth evaluation on the energy, carbon emissions, and economic performance of the [C_2H_8N][TfO]-based ED process.

3.1. Process simulation

Table 6 gives the composition of crude feed 1 (flow rate 26066 kg/h) and crude feed 2 (flow rate 5279 kg/h). The data and information of these two feed streams are directly obtained from a China's oil refinery, where the conventional EB distillation process, as presented in Fig. 2, is currently used. In this work, the rigorous equilibrium stage model (RADFRAC) is employed to simulate all involved columns including DC, EDC, and SRC for achieving accurate simulation results. In addition, the SRK and UNIFAC [59] models are, respectively, employed to perform the thermodynamic calculations for the EB distillation process simulation [60].

Parameter optimization that allows us to maximize the process performance is an important step to simulate the process in Aspen Plus. In this study, several sensitivity analyses are employed to optimize the key design and operation. The optimizing strategy used in our work is shown in Fig. S1. The optimization of the parameters (i.e. the number of equilibrium stages, feeding location, reflux ratio) of the conventional EB distillation process is performed on the basis of the actual requirements in the industry. The parameter optimization results are given in Table 7. Obviously, the benzene column and ethylbenzene column account for the most energy consumption of the whole EB distillation process.

For the [C_2H_8N][TfO]-based EB distillation process that includes three extractive distillation columns (EDC1-3) and a SRC, the key parameters will be analyzed as follows: (1) the number of equilibrium stages(N_{ST}), feeding location, and RR of EDC1-3; (2) N_{ST} and feed location of SRC and RR; (3) Mass flow rate of extractant in EDC1; (4) Distillation column pressure of EDC1 and EDC2. In EDC1, as the N_{ST}

Table 6
Composition of the crude feeds for EB distillation process in a China's oil refinery.

	Components	Molecular formulas	wt. %	mol %
Crude feed 1	AIR	AIR	0.063	0.179
	CARBON-MONOXIDE	CO	0.006	0.018
	CARBON-DIOXIDE	CO_2	0.07	0.131
	METHANE	CH_4	0.03	0.153
	ETHANE	C_2H_6	0.121	0.330
	ETHYLENE	C_2H_4	0.001	0.003
	N-BUTANE	C_4H_{10}-1	0.006	0.008
	1-BUTENE	C_4H_8-1	0.001	0.001
	N-PENTANE	C_5H_{12}-1	0.028	0.032
	N-HEXANE	C_6H_{14}-1	0.055	0.052
	BENZENE	C_6H_6	80.806	84.837
	N-HEPTANE	C_7H_{16}-1	0.096	0.079
	TOLUENE	C_7H_8	0.032	0.029
	ETHYLBENZENE	C_8H_{10}-4	16.86	13.024
	P-XYLENE	C_8H_{10}-3	0.016	0.012
	ISOPROPYLBENZENE	C_9H_{12}-2	0.099	0.068
	O-DIETHYL BENZENE	$C_{10}H_{14}$-2	1.698	1.038
	1,2,4-TRIETHYLBENZENE	$C_{12}H_{18}$-6	NA	NA
	N-BUTYLBENZENE	*N*-BUT-02	0.011	0.007
	N-PENTYLBENZENE	$C_{11}H_{16}$	NA	NA
Crude feed 2	*N*-PENTANE	C_5H_{12}-1	0.062	0.071
	N-HEXANE	C_6H_{14}-1	0.062	0.059
	BENZENE	C_6H_6	83.655	88.062
	N-HEPTANE	C_7H_{16}-1	0.107	0.088
	TOLUENE	C_7H_8	0.038	0.034
	ETHYLBENZENE	C_8H_{10}-4	11.354	8.794
	O-DIETHYL BENZENE	$C_{10}H_{14}$-2	4.692	2.874
	1,2,4-TRIETHYLBENZENE	$C_{12}H_{18}$-6	NA	NA
	N-BUTYLBENZENE	*N*-BUT-02	0.03	0.018
	N-PENTYLBENZENE	$C_{11}H_{16}$	NA	NA

Table 7
Optimized parameters of the conventional EB distillation process.

	Benzene column (DC1)	Ethylbenzene column (DC2)	Diethyl benzene column (DC3)
Number of equilibrium stages	100	60	30
Feed location	28/36	50	10
Reflux ratio (RR)	1.4	5	10
Column mass flow rate (kg/h)	25420.8 / 5924.2	5183.6 / 740.5	74 / 666.5
Reboiler heat utility (kW)	6188.3	2649.4	66.3
Percentage of energy consumption	69.5 %	29.8 %	0.7 %

changes from 90 to 110, the mass ratio of solvent (S/F) begins to decrease rapidly and then maintains a relatively gentle trend. When the N_{ST} is 104, the solvent ratio is the smallest, as shown in Fig. 3(a). Therefore, the N_{ST} of EDC1 is determined to be 104. In EDC2, with the increase of the N_{ST}, RR shows a decreasing trend first and then maintaining a gentle trend, as shown in Fig. 3(b), so the optimal N_{ST} is set as 60. Fig. 3(c) and 3(d) illustrate the impact of the N_{ST} on the RR of EDC3 and SRC, respectively. It is finally determined that 25 equilibrium stages are applied for EDC3 and 30 equilibrium stages for SRC. The material balance of the conventional and $[C_2H_8N][TfO]$-based ED processes are shown in Table S1 and S2.

Figs. 4-7 present the details of the sensitivity analysis on the main process parameters in EDC1-3 and SRC, respectively. In our previous study, it was found that the heat duty of the distillation column increases with increasing the feed temperature [50], so the effect of the feed temperature on the process performance is excluded from consideration in this work. The effect of the feed location of S1 and S2 on the RR, reboiler duty, and condenser duty of EDC1 are given in Fig. 4. We find that EDC1 has the smallest RR and the lowest heat duty when the feed location of S1 is 37 and the feed location of S2 is 33. In EDC2, both the RR and heat duty of the reboiler decrease and then increase with increasing feed location, as shown in Fig. 5. This column demands the smallest heat duty input when the feed location is set to 45. In EDC3, firstly, the RR decreases slightly. And then increases significantly with increasing feed location, as illustrated in Fig. 6. The optimal energy performance of this column is identified with a feed location of 5. For the SRC, both the RR and the heat duty of the reboiler have similar trends against the feed location in EDC3, as presented in Fig. 7, and the optimal feed location of this column is 7. In all distillation columns, the heat duty of the condenser shows the opposite trend to the RR and the heat duty of the reboiler.

Similar to the conventional EB distillation process, the extractive distillation benzene column (EDC1) accounts for most energy consumption of the whole $[C_2H_8N][TfO]$-based EB distillation process. Therefore, the key parameters of this distillation column are further investigated, and the results are presented in Figs. 8-10. Table 8 gives all the optimized key design parameters of the IL-based EB distillation processes. It should be pointed out that the operating pressure of SRC is controlled to ensure that the maximum operating temperature is lower than the thermal decomposition temperature of IL.

3.2. Energy consumption analysis and economic evaluation

The Aspen Energy Analyzer V9 and Aspen Process Economics Analyzer V9 will be employed to evaluate the energy, carbon emission, and economic performance of the conventional and $[C_2H_8N][TfO]$-based EB distillation processes.

3.2.1. Energy consumption analysis

The analysis of energy consumption should be considered to evaluate process performance, especially for an energy-intensive process, such as the EB distillation process. Due to the advantages of IL solvent, the energy performance of the distillation columns in the suggested IL-based EB distillation process is better than that of the conventional process. As presented in Fig. 11, the hot utilities of DCs in the conventional process is over 8.9 MW, while the total hot utilities of EDCs and SRC in the $[C_2H_8N][TfO]$-based ED process is about 5.3 MW, leading to a 40 % energy-savings.

The pinch technology is a powerful method to achieve maximum heat recovery in the heat exchangers network (HEN). In our study, the optimal HEN scenarios of both the conventional and $[C_2H_8N][TfO]$-based EB distillation processes are carried out to maximize heat recovery. The hot and cold streams used in the HNE design are directly taken from Aspen Plus V9. The supply, target temperature, and heat capacity of all process streams are listed in Table S3. The heat transfer and cost coefficients embedded in the Aspen database are used in the heat integration. The total annual cost (TAC) is used to evaluate and analyze the performance of the proposed HENs. With a ΔT_{min} of 10 K, the pinch temperatures of the conventional and $[C_2H_8N][TfO]$-based EB distillation processes are 475.45 K and 415.45 K, respectively. The grand composite curves (GCC) and the grid diagrams of recommended HENs for the above two separation processes are given in Figs. S2 and S3, respectively. The summary of the optimized HENs for both the conventional and $[C_2H_8N][TfO]$-based EB distillation processes is presented in Table 9. The TAC of the optimized HEN is less than that of the initial HEN. It because there is the cold utility utilization in series employed in the optimized HEN as shown in Fig. S3.

For the optimized HEN designs, the minimum heating and cooling duties in the $[C_2H_8N][TfO]$-based EB distillation process are, respectively, reduced by 41 % and 39 % when compared with the conventional EB distillation process, as shown in Table 9. Meanwhile, the $[C_2H_8N][TfO]$-based separation process saves 39 % in operating costs (OPEX) and 25 % in capital costs. As a result, TAC of 37 % is reduced. Overall,

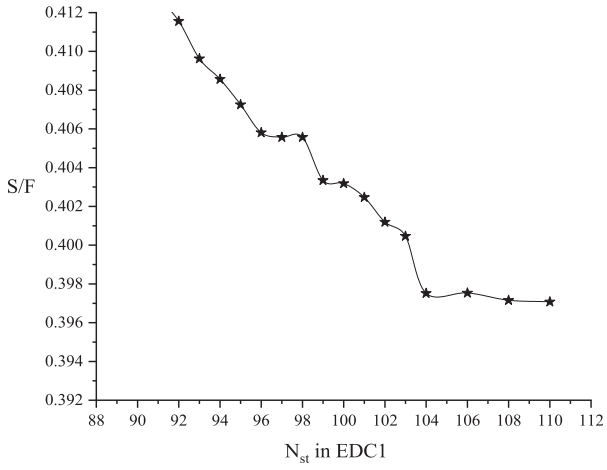

(a) Extractive distillation benzene column

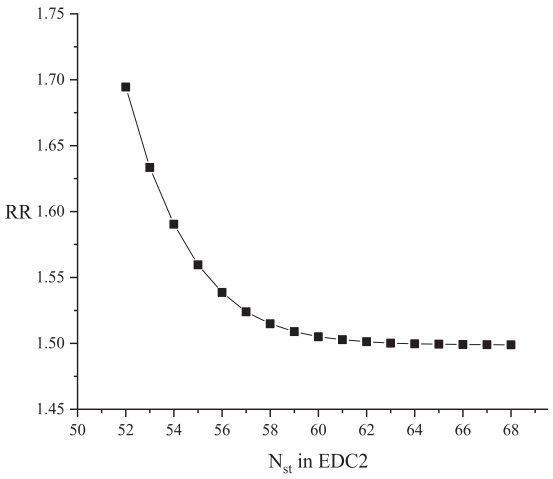

(b) Extractive distillation ethylbenzene column

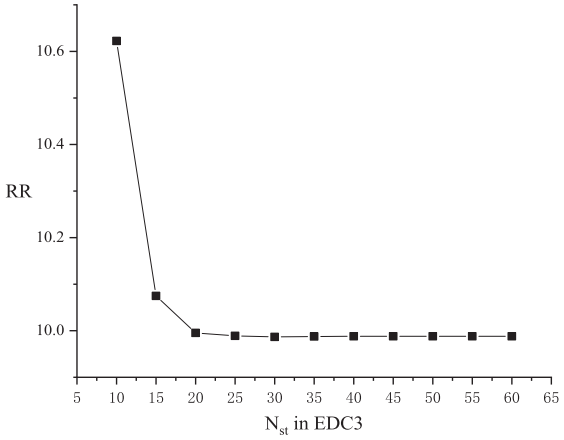

(c) Extractive distillation diethyl benzene column

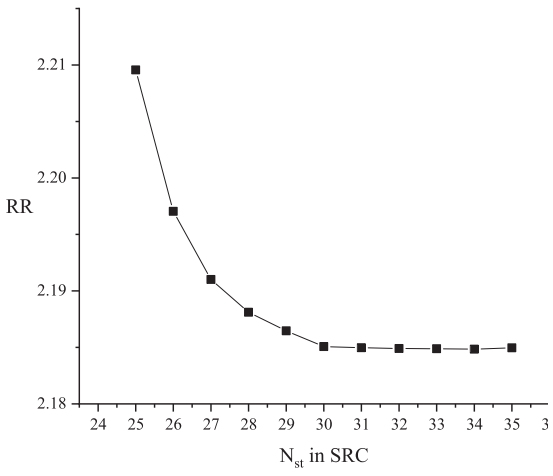

(d) Solvent recovery column

Fig. 3. Relationship between the S/F, RR, and the N_{ST}.

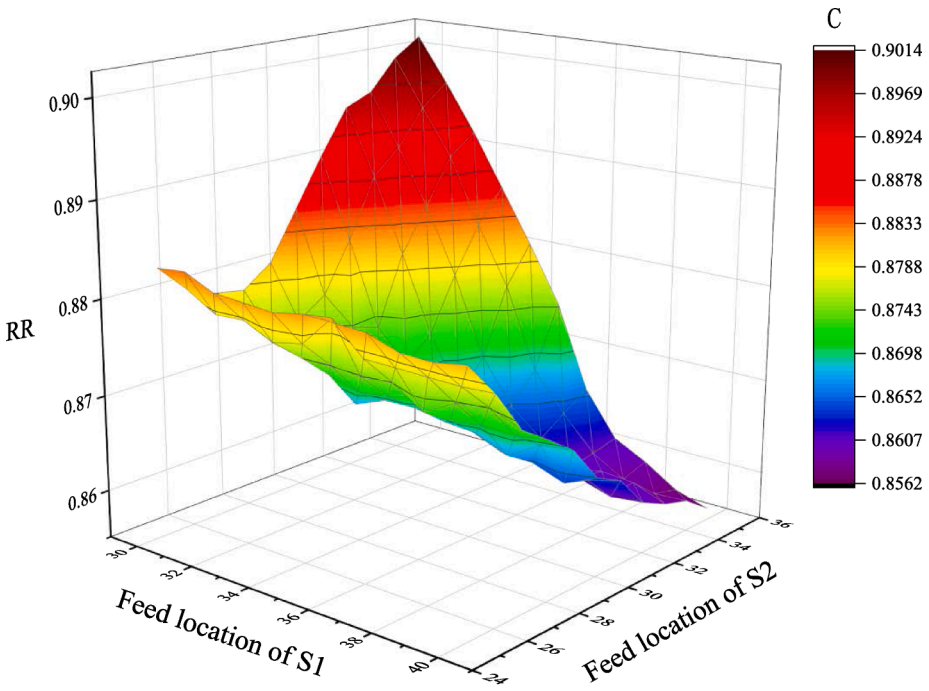

(a)

Fig. 4. Sensitivity analysis on the main design and operation parameters in extractive distillation benzene column.

the energy efficiency of the $[C_2H_8N][TfO]$-based EB distillation process is much higher than that of the conventional EB distillation process. Moreover, if heat integration is considered, the capital cost and TAC of the conventional process and the $[C_2H_8N][TfO]$-based process are reduced by 21 % and 36 %, respectively. The results indicate that heat integration between cold and hot streams is essential in the process design.

Total energy consumption (TEC) contains several energy mediums used in hot and cold utilities. In our work, the equivalent energy penalty is used to calculate the TEC of the studied EB distillation processes. The equivalent energy penalty of used working mediums can be found in Table S4. In addition, specific energy consumption (*SEC*), as expressed by Eq.13, is an effective index for evaluating the quality of TEC and it will be used to compare the energy performance between the conventional and IL-based EB distillation processes.

$SEC = \frac{TEC}{m_{EB}}$(13)where the unit of *SEC* is MJ/kg EB and the unit of TEC is MJ/h. m_{EB} is the mass basis flow of EB product distilled from the top of EDC2. The TEC of the conventional EB distillation process has two components: AIR and HP Steam. For the IL-based ethylbenzene distillation process, the TEC contains AIR, Fired Heat, and HP Steam. As illustrated in Fig. 12, the *SEC* of the conventional EB distillation process is 14.5 MJ/kg EB, and for the $[C_2H_8N][TfO]$-based EB distillation process the value is 8.8. In addition, the IL-based EB separation process saves 40 % heating facility and 39 % cooling facility, resulting in a 39 % reduction in *SEC*, compared to the conventional EB distillation process.

3.2.2. Environmental assessment

For the distillation process, environmental friendliness can be evaluated by calculating CO_2 emissions [61]. The Net CO_2 emission is calculated in Eq. 14 [62].

$$\text{Net } CO_2 \text{ emission} = \text{Direct emission} + \text{Indirect emission} - \text{Captured } CO_2 \quad (14)$$

In this study, no part of the process products contains CO_2, so direct emissions are not calculated. Indirect emissions are from utilities and can be obtained directly through Aspen Plus. Compared with the conventional EB process, the $[C_2H_8N][TfO]$-based EB distillation process has a makeup ionic liquid as the material input. The amount of the makeup ionic liquid is only 0.23 kg/h, and the CO2 emission is 1.073 kg/h [63], which is very small compared with the indirect emissions by utilities, we have omitted this part of CO_2 emissions. The carbon emission results of the conventional and $[C_2H_8N][TfO]$-based EB distillation process are shown in Fig. 13. The $[C_2H_8N][TfO]$-based EB distillation process has almost less 40 % carbon emissions than the conventional EB distillation process.

3.2.3. Economic evaluation

In general, economic performance is the most important indicator for the acceptance and implementation of new processing technology in industrial-scale production. TAC combining the annualized capital cost (ACC) and the total OPEX is a well-known indictor that can be directly used in the economic evaluation of a process. The information required to calculate the ACC for different equipment (i.e. mathematical models, model parameters) is given in Table S7. Due to the introduction of IL solvent, the cost of IL regeneration and recycling is the non-negligible part of ACC for the EB distillation process involving IL, while the cost of make-up IL is classified as a contribution of OPEX. Therefore, the TAC is obtained to evaluate the proposed process [19,59].

The price of ILs would definitely affect the TAC of the IL-based process. In this case, the price of $[C_2H_8N][TfO]$ is assumed to be 50 $/kg from continuous production [59,64]. Fig. 14 presents the detailed economic performance of the conventional and $[C_2H_8N][TfO]$-based EB distillation processes. The ACC increased by 19 % and OPEX decreased by 22 % compared with the conventional EB distillation process. The increase in ACC is due to the configuration for the heating furnace as the reboiler of SRC in the $[C_2H_8N][TfO]$-based EB distillation process compared with the conventional EB distillation process. However, the

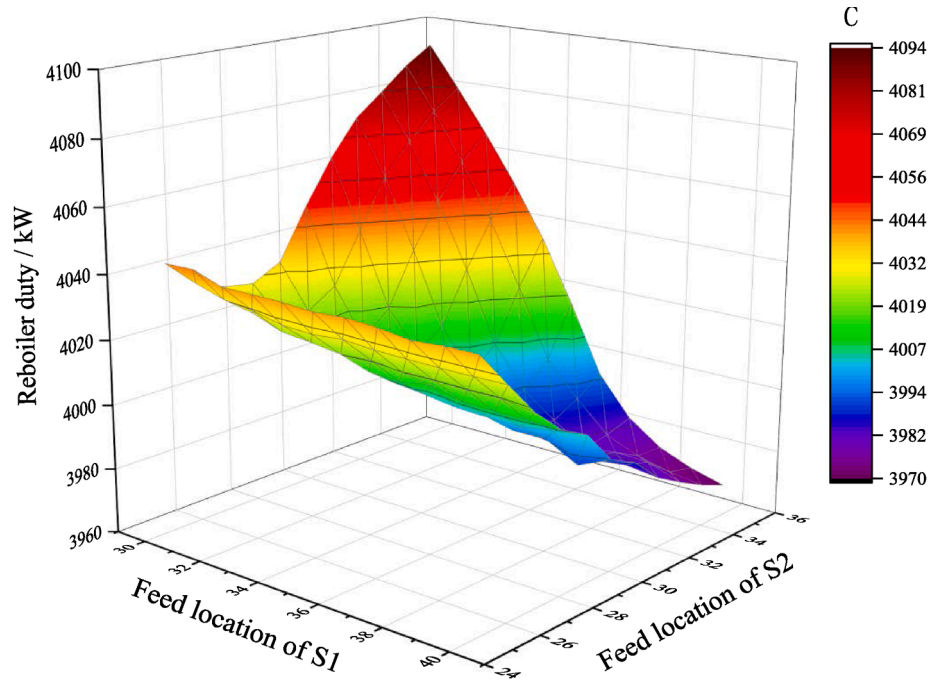

(b)

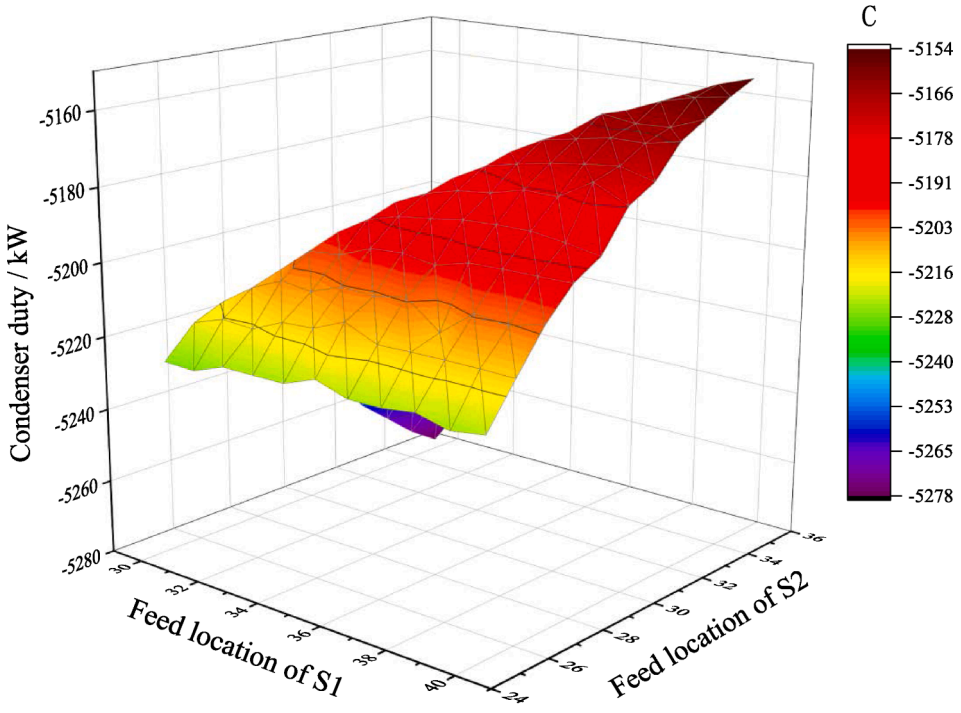

(c)

Fig. 4. (*continued*).

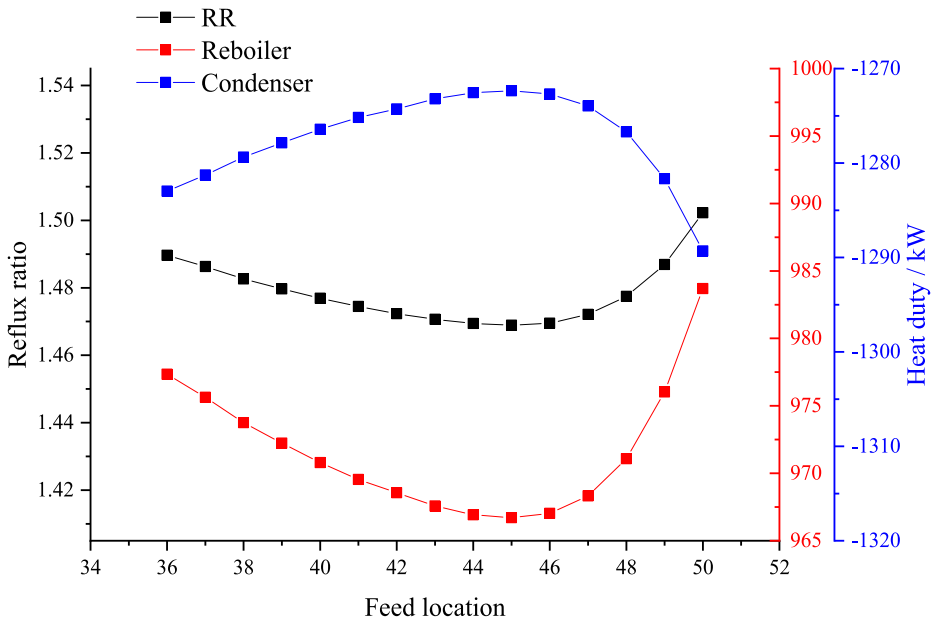

Fig. 5. Sensitivity analysis on the main design and operation parameters in extractive distillation ethylbenzene column.

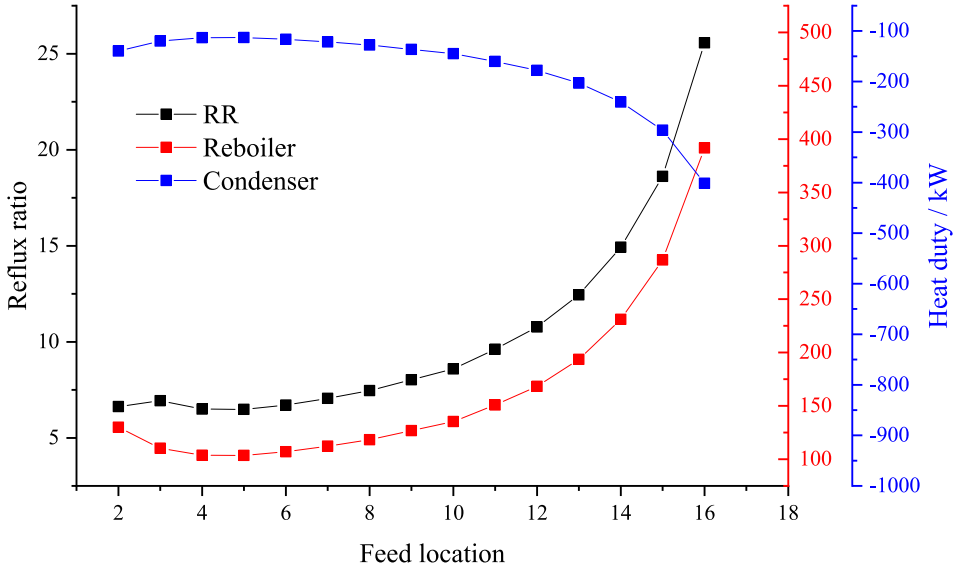

Fig. 6. Sensitivity analysis on the main design and operation parameters in extractive distillation diethyl benzene column.

TAC has decreased by 11 % because of 40 % energy conversation in the [C_2H_8N][TfO]-based EB distillation process. Besides, it is found that the contribution of OPEX in TAC is greater than ACC for both two processes, indicating the importance of operating parameters optimization in process design.

Although the price of IL has higher than that of many traditional organic solvents, in the proposed IL-based EB distillation process, the cost of make-up IL per year is 123,256 $/y, which only accounts for 6 % of OPEX. However, the price of ILs also has a major impact on the economic performance of the proposed IL-based EB distillation process [40]. Therefore, the marginal price of the screened IL (P_m@$TAC_{conventional\ process}$ = $TAC_{IL\text{-}based\ process}$) is presented as an evaluating factor to assess the economic benefit of this [C_2H_8N][TfO]-based separation process [19]. In this work, the marginal price of [C_2H_8N][TfO] is 2349 $/kg for the IL-based EB distillation process, showing the good competitiveness of this new separation technology. In addition, the wide temperature interval of process streams in the [C_2H_8N][TfO]-based process means that heat integration with adjacent plants can be employed to achieve better performance of the HEN, which can lead to further energy and economic benefit improvement of this process.

4. Conclusion

This work proposes an IL-based EB distillation process for achieving energy-efficient and low-carbon-emission EB production from dry gas. In this process, the structure of task-specific ILs is optimized by maximizing a mass-based separation performance design target in a CAILD-based MINLP mathematical model. An ammonium-based IL [C_2H_8N]

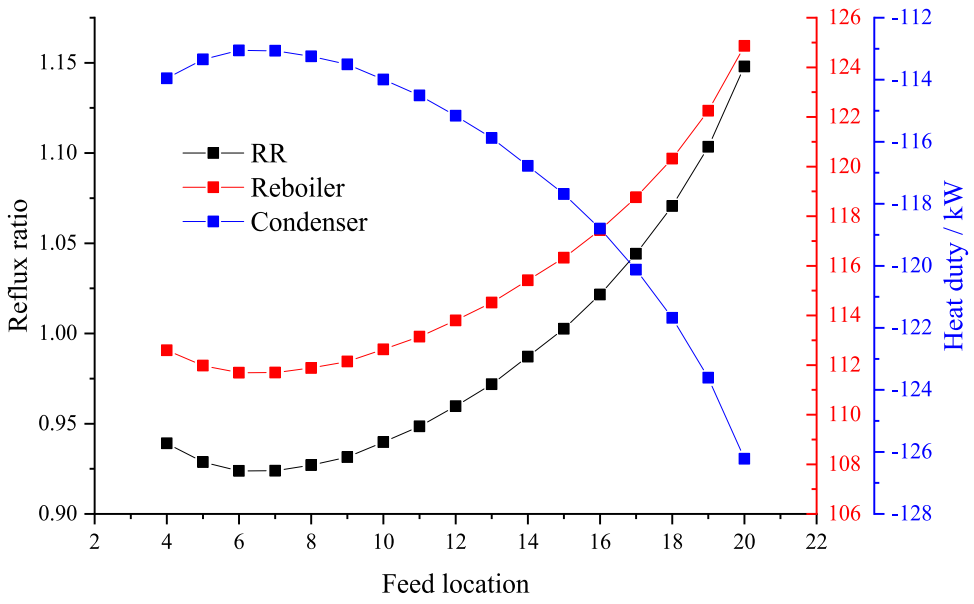

Fig. 7. Sensitivity analysis on the main design and operation parameters in solvent recovery column.

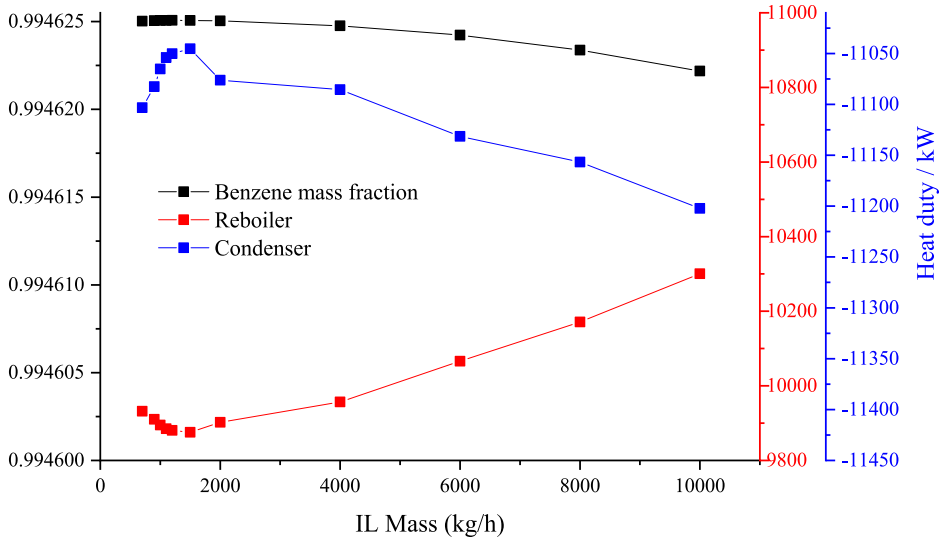

Fig. 8. Sensitivity analysis of IL mass flow rates.

[TfO] is identified as the best performing candidate that can meet the requirements in all distillation columns. The employment of this IL-based separation technology is demonstrated through a case study in China's oil refining industry. The results from the process rigorous simulation and complete optimization indicate that both the conventional and $[C_2H_8N][TfO]$-based distillation processes can obtain high-purity products (99.4 % benzene, 96 % ethylbenzene, 99.3 % diethylbenzene). However, results of process evaluation show that the $[C_2H_8N][TfO]$-based EB distillation process has much better process performance than that of the conventional process. When compared to the conventional distillation process, the $[C_2H_8N][TfO]$-based EB distillation process saves 40.2 % heating utility and 38.8 % cooling utility. Meanwhile, the $[C_2H_8N][TfO]$-based EB distillation process is able to reduce 40 % of carbon emissions. In addition, the $[C_2H_8N][TfO]$-based EB distillation process can show 21 % OPEX savings, leading to a 11 % reduction in TAC.

In this work, the OPEX contributes more than ACC in TAC for both the conventional and the $[C_2H_8N][TfO]$-based EB distillation processes, indicating the importance of heat integration with maximum heat recovery. On the other hand, the marginal price of $[C_2H_8N][TfO]$ (2349 $/kg) is much higher than the reference price (50 $/kg) from bulk production, indicating a very low investment risk of this separation technology. To the best of our knowledge, most ILs currently used in the industry are ammonium-based ILs. This happens as they generally have better thermal stability than other ILs, such as imidazolium- and pyridinium-based ILs, which would definitely enhance the feasibility of the $[C_2H_8N][TfO]$-based distillation technology. In addition, although this work focuses on the EB distillation process, the process design and optimization can be applied to other high energy-consuming separations, where the mixture generally contains benzene homologs with similar properties, such as benzene and styrene.

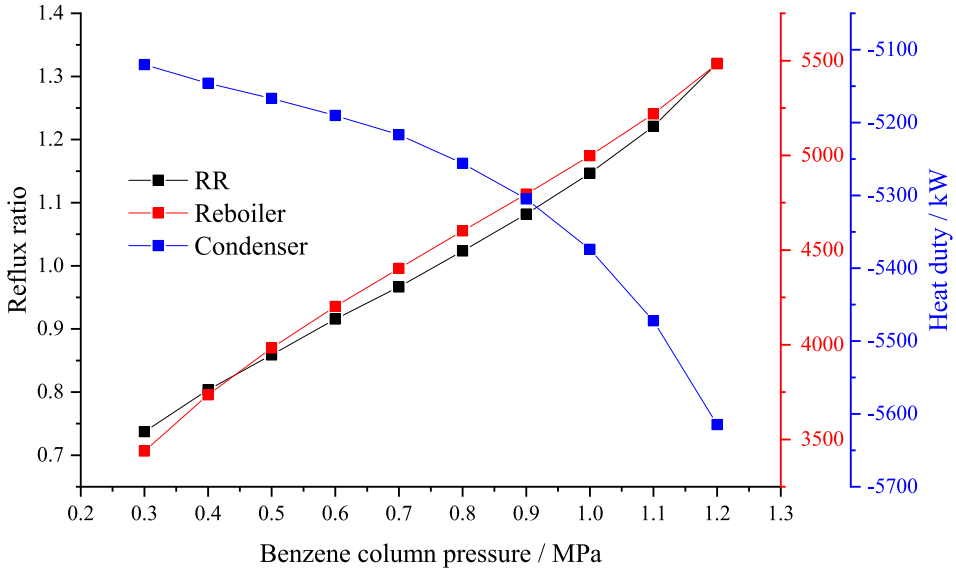

（a）

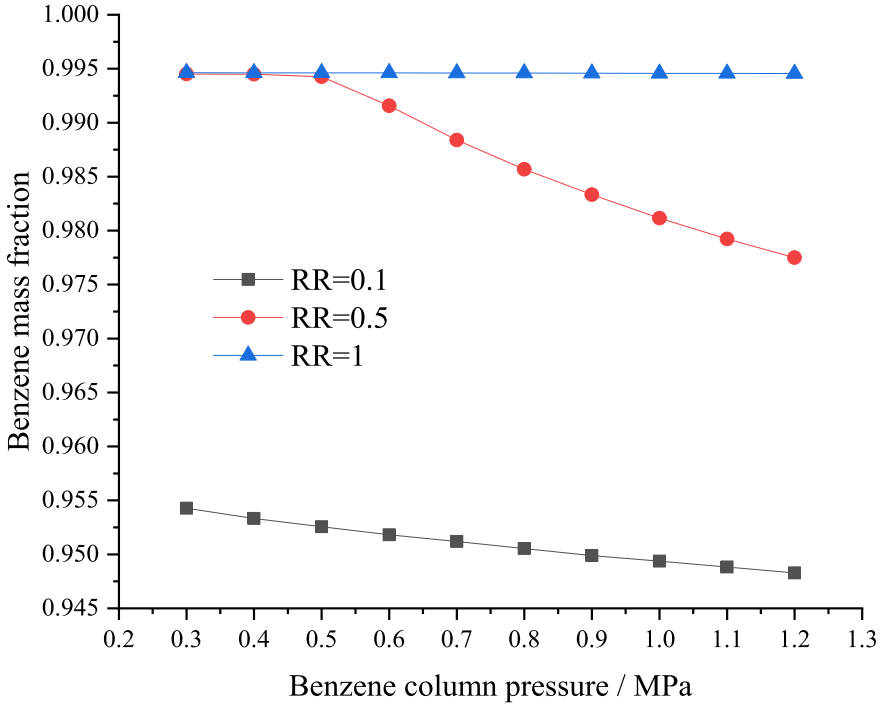

（b）

Fig. 9. Sensitivity analysis of benzene column pressure.

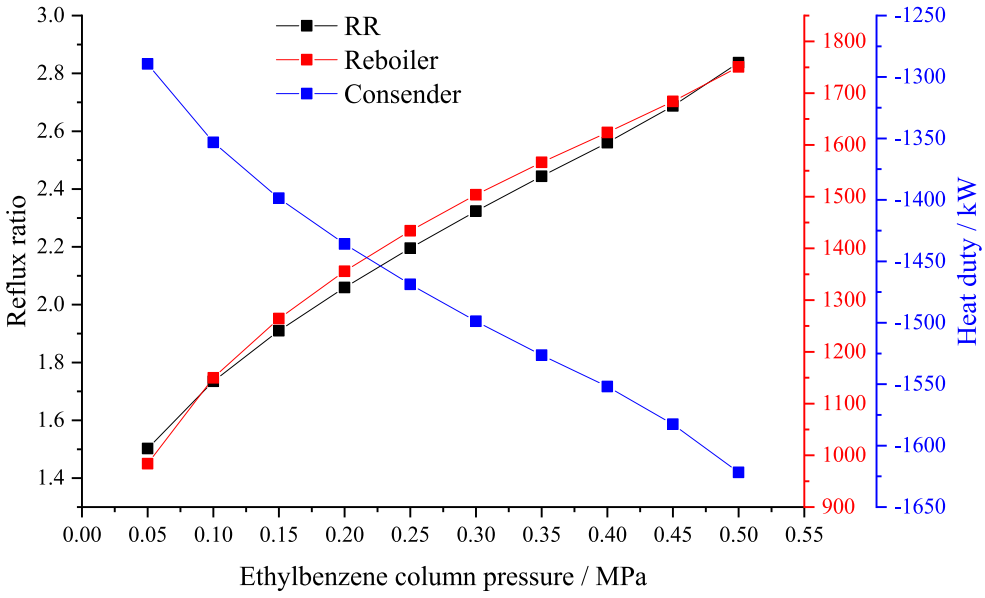

(a)

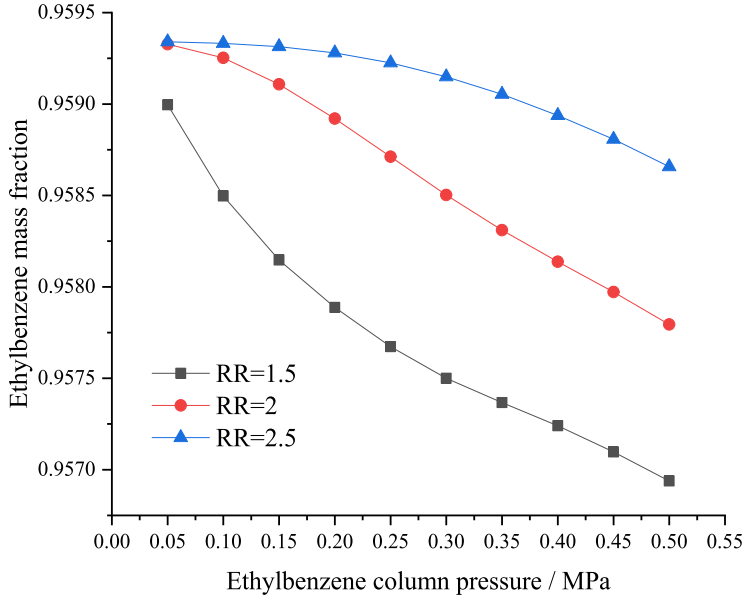

(b)

Fig. 10. Sensitivity analysis of ethylbenzene column pressure.

Table 8
Optimized key operating parameters of the IL-based EB distillation process.

Column	EDC1	EDC2	EDC3	SRC
Number of equilibrium Stages	104	60	25	30
Feed location	33/37	45	5	7
Column top pressure /MPa	0.5	0.05	0.03	0.01
RR	0.86	1.48	10	2

CRediT authorship contribution statement

Yang Lei: Conceptualization, Methodology, Writing – original draft. **Zhaoyang Yu:** Data curation. **Zhiqiang Wei:** Data curation. **Xinyan Liu:** Formal analysis, Supervision. **Haoshui Yu:** Data curation. **Xiaodong Liang:** Formal analysis. **Georgios M. Kontogeorgis:** Supervision. **Yuqiu Chen:** Supervision.

Declaration of Competing Interest

The authors declare that they have no known competing financial interests or personal relationships that could have appeared to influence the work reported in this paper.

Data availability

No data was used for the research described in the article.

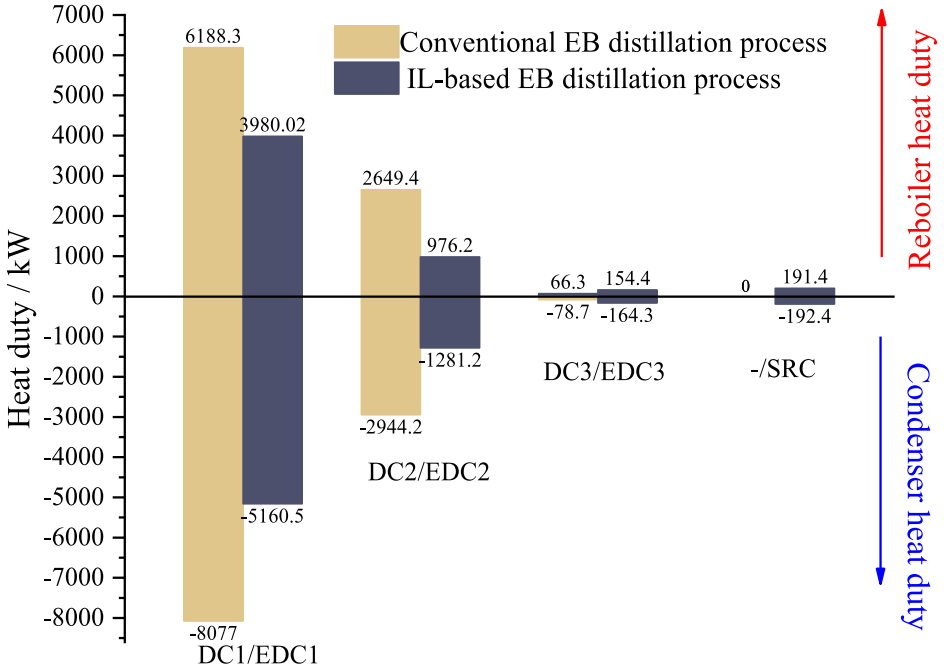

Fig. 11. Hot and cold utilities of all columns in two processes.

Table 9
Pinch analysis and process performance of the EB distillation process with an optimized HEN design.

Items	Conventional EB distillation process			$[C_2H_8N][TfO]$-based EB distillation process		
	Targets	HEN performance	Percent of target (%)	Targets	HEN performance	Percent of target (%)
Hot utilities (MJ/h)	3.21×10^4	3.21×10^4	100	1.91×10^4	1.91×10^4	100
Cold utilities (MJ/h)	3.99×10^4	3.99×10^4	100	2.44×10^4	2.44×10^4	100
	Cost index targets	Network indexes	Percent of target (%)	Cost index targets	Network cost indexes	Percent of target (%)
OPEX ($/s)	2.22×10^{-2}	2.22×10^{-2}	100	1.36×10^{-2}	1.36×10^{-2}	100
Capital cost ($)	4.09×10^5	3.74×10^5	91.3	3.23×10^5	2.80×10^5	86.69
TAC ($/s)	2.56×10^{-2}	2.54×10^{-2}	98.9	1.63×10^{-2}	1.59×10^{-2}	97.8
Number of heat exchanges	8	8				

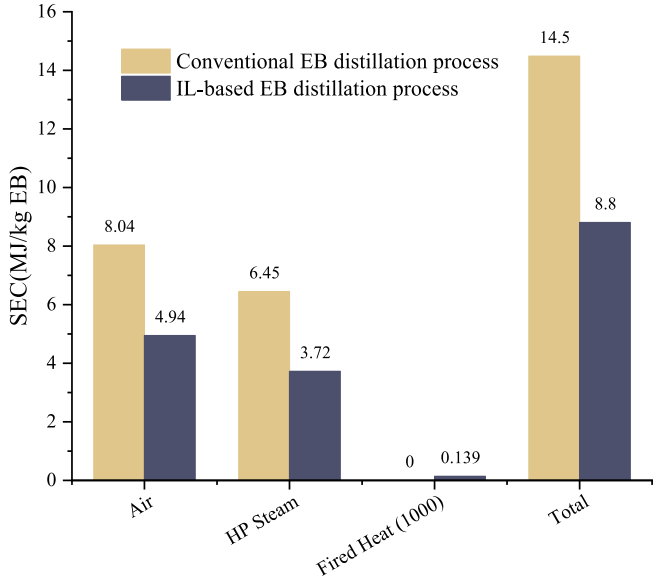

Fig. 12. Specific energy consumption in two processes.

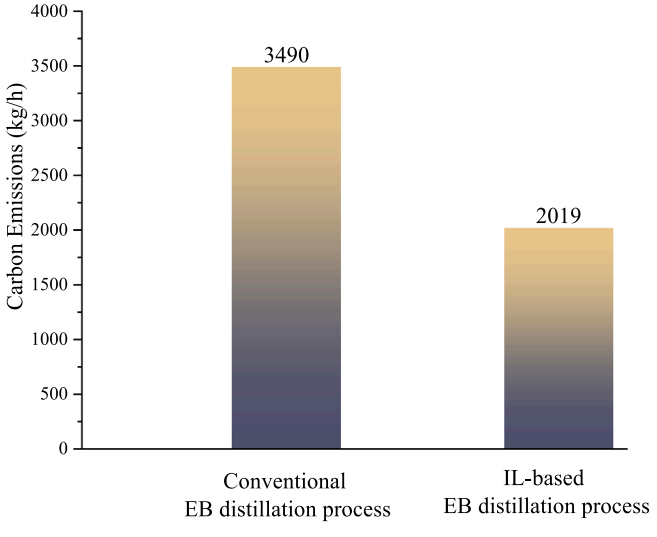

Fig. 13. CO_2 emission analysis in two processes.

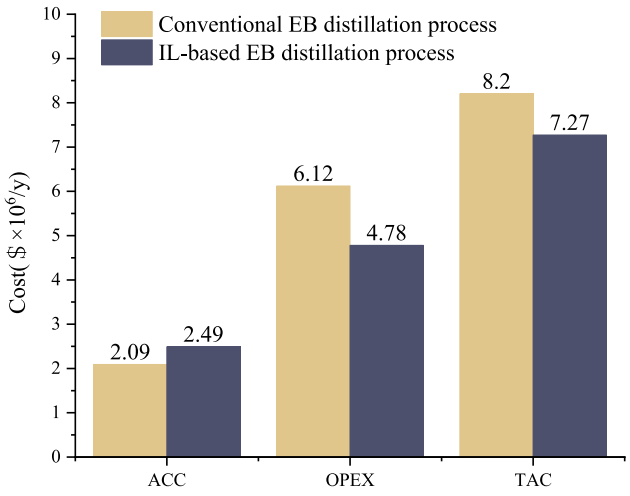

Fig. 14. Comparison of total cost (TAC) in two processes.

Acknowledgments

The authors gratefully acknowledge the financial support from the National Natural Science Foundation of China (21706198) and the Hubei Province Undergraduate Training Program for Innovation and Entrepreneurship (S202110488034, S202210488116X).

Appendix A. Supplementary material

Supplementary data to this article can be found online at https://doi.org/10.1016/j.seppur.2022.122827.

References

[1] Z. Zhao, W. Li, Y. Dai, G. Ge, X. Guo, G. Wang, Carbon nitride encapsulated nanodiamond hybrid with improved catalytic performance for clean and energy-saving styrene production via direct dehydrogenation of ethylbenzene, ACS Sustain. Chem. Eng. 3 (12) (2015) 3355–3364.
[2] W.L. Luyben, Design and control of the ethyl benzene process, AIChE J. 57 (3) (2011) 655–670, https://doi.org/10.1002/aic.12289.
[3] Y. Wu, D. Meng, D. Yao, et al., Mechanism analysis, economic optimization, and environmental assessment of hybrid extractive distillation–pervaporation processes for dehydration of n-propanol, ACS Sustain. Chem. Eng. 8 (11) (2020) 4561-4571. https://doi.org/10.1021/acssuschemeng.0c00263.
[4] S. Widagdo, W.D. Seider, Journal review. Azeotropic distillation, AIChE J. 42 (1996) 96–130, https://doi.org/10.1002/aic.690420110.
[5] M.F. Malone, M.F. Doherty, Reactive distillation, Ind. Eng. Chem. Res. 39 (11) (2000) 3953–3957, https://doi.org/10.1016/S1351-4180(04)00503-3.
[6] D. Cai, Y. Xie, L. Li, J. Ren, X. Lin, T. Qiu, Design and synthesis of novel Brønsted-Lewis acidic ionic liquid and its application in biodiesel production from soapberry oil, Energ. Convers. Manage. 166 (2018) 318–327.
[7] R. Vijayaraghavan, D.R. Macfarlane, CO_2-based alkyl carbamate ionic liquids as distillable extraction solvents, ACS Sustain. Chem. Eng. 2 (7) (2014) 1724–1728, https://doi.org/10.1021/sc5002066.
[8] X. Chen, S. Ming, X. Wu, C. Chen, C. Asumana, G. Yu, Cu(I)-based ionic liquids as potential absorbents to separate propylene and propane, Sep. Sci. Technol. 48 (15) (2013) 2317–2323.
[9] Z. Lei, C. Li, B. Chen, Extractive distillation: a review, Separat. Purificat. Rev. 32 (2) (2003) 121–213.
[10] M. Ayuso, P. Navarro, C. Moya, D. Moreno, J. Palomar, J. García, F. Rodríguez, Extractive distillation with ionic liquids to separate benzene, toluene, and xylene from pyrolysis gasoline: process design and techno-economic comparison with the morphylane process, Ind. Eng. Chem. Res. 61 (6) (2022) 2511–2523.
[11] P. Navarro, I. de Dios-García, M. Larriba, N. Delgado-Mellado, M. Ayuso, D. Moreno, J. Palomar, J. García, F. Rodríguez, Dearomatization of pyrolysis gasoline by extractive distillation with 1-ethyl-3-methylimidazolium tricyanomethanide, Fuel. Process. Technol. 195 (2019) 106156, https://doi.org/10.1016/j.fuproc.2019.106156.
[12] X. Liu, Y. Chen, S. Zeng, X. Zhang, S. Zhang, X. Liang, R. Gani, G.M. Kontogeorgis, Structure optimization of tailored ionic liquids and process simulation for shale gas separation, AIChE J. 66 (2) (2020), https://doi.org/10.1002/aic.16794.
[13] X. Liu, Y. Chen, S. Zeng, X. Zhang, X. Liang, R. Gani, G.M. Kontogeorgis, Separation of NH_3/CO_2 from melamine tail gas with ionic liquid: process evaluation and thermodynamic properties modelling, Sep. Purif. Technol. 274 (2021) 119007, https://doi.org/10.1016/j.seppur.2021.119007.
[14] Y. Chen, N. Garg, H. Luo, G.M. Kontogeorgis, J.M. Woodley, Ionic liquid-based in situ product removal design exemplified for an acetone-butanol-ethanol fermentation, Biotechnol. Progr. 37 (5) (2021), https://doi.org/10.1002/btpr.3183.
[15] N.L. Mai, Y.M. Koo, Computer-aided design of ionic liquids for high cellulose dissolution, ACS Sustain. Chem. Eng. 4 (2) (2016) 541–547, https://doi.org/10.1021/acssuschemeng.5b00958.
[16] Y. Chen, R. Gani, G.M. Kontogeorgis, J.M. Woodley, Integrated ionic liquid and process design involving azeotropic separation processes, Chem. Eng. Sci. 203 (2019) 402–414.
[17] Z. Song, C. Zhang, Z. Qi, T. Zhou, K. Sundmacher, Computer-aided design of ionic liquids as solvents for extractive desulfurization, AIChE J. 64 (3) (2018) 1013–1025.
[18] Z. Song, X. Li, H.e. Chao, F. Mo, T. Zhou, H. Cheng, L. Chen, Z. Qi, Computer-aided ionic liquid design for alkane/cycloalkane extractive distillation process, Green Energy Environ. 4 (2) (2019) 154–165.
[19] Y. Lei, Y. Zhou, Z. Wei, Y. Chen, F. Guo, W. Yan, Optimal design of an ionic liquid (IL)-based aromatic extractive distillation process involving energy and economic evaluation, Ind. Eng. Chem. Res. 60 (9) (2021) 3605–3616.
[20] Z. Lei, J. Zhang, Q. Li, B. Chen, UNIFAC model for ionic liquids, Ind. Eng. Chem. Res. 48 (5) (2009) 2697–2704.
[21] S. García, M. Larriba, J. García, J.S. Torrecilla, F. Rodríguez, Alkylsulfate-based ionic liquids in the liquid–liquid extraction of aromatic hydrocarbons, J. Chem. Thermodyn. 45 (1) (2012) 68–74.
[22] A. Arce, M.J. Earle, S.P. Katdare, H. Rodríguez, K.R. Seddon, Application of mutually immiscible ionic liquids to the separation of aromatic and aliphatic hydrocarbons by liquid extraction: a preliminary approach, Phys. Chem. Chem. Phys. 10 (18) (2008) 2538, https://doi.org/10.1039/b718101a.
[23] A.B. Pereiro, A. Rodriguez, Application of the ionic liquid Ammoeng 102 for aromatic/aliphatic hydrocarbon separation, J. Chem. Thermodyn. 41 (8) (2009) 951–956, https://doi.org/10.1016/j.jct.2009.03.011.
[24] A. Arce, M.J. Earle, H. Rodríguez, K.R. Seddon, A. Soto, Bis{(trifluoromethyl) sulfonyl}amide ionic liquids as solvents for the extraction of aromatic hydrocarbons from their mixtures with alkanes: effect of the nature of the cation, Green. Chem. 11 (3) (2009) 365–372.
[25] C.V. Manohar, T. Banerjee, K. Mohanty, Co-solvent effects for aromatic extraction with ionic liquids, J. Mol. Liq. 180 (2013) 145–153, https://doi.org/10.1016/j.molliq.2013.01.019.
[26] M. Ayuso, A. Cañada-Barcala, M. Larriba, P. Navarro, N. Delgado-Mellado, J. García, F. Rodríguez, Enhanced separation of benzene and cyclohexane by homogeneous extractive distillation using ionic liquids as entrainers, Sep. Purif. Technol. 240 (2020) 116583, https://doi.org/10.1016/j.seppur.2020.116583.
[27] I. Díaz, J. Palomar, M. Rodríguez, J. de Riva, V. Ferro, E.J. González, Ionic liquids as entrainers for the separation of aromatic–aliphatic hydrocarbon mixtures by extractive distillation, Chem. Eng. Res. Des. 115 (2016) 382–393.
[28] I. Domínguez, N. Calvar, E. Gómez, Á. Domínguez, Liquid–liquid extraction of aromatic compounds from cycloalkanes using 1-butyl-3-methylimidazolium methylsulfate ionic liquid, J. Chem. Eng. Data. 58 (2) (2013) 189–196.
[29] M.R. Heidari, B. Mokhtarani, N. Seghatoleslami, A. Sharifi, M. Mirzaei, Liquid–liquid extraction of aromatics from their mixtures with alkanes using 1-methyl 3-octylimidazolium thiocyanate ionic liquid, J. Chem. Thermodyn. 54 (2012) 310–315.
[30] S.A. Sakal, Y.-Z. Lu, X.-C. Jiang, C. Shen, C.-x. Li, A promising ionic liquid [BMIM] $[FeCl_4]$ for the extractive separation of aromatic and aliphatic hydrocarbons, J. Chem. Eng. Data. 59 (3) (2014) 533–539.
[31] A. Arce, M.J. Earle, H. Rodríguez, K.R. Seddon, Separation of aromatic hydrocarbons from alkanes using the ionic liquid 1-ethyl-3-methylimidazolium bis (trifluoromethyl) sulfonyl amide, Green Chem. 9 (1) (2007) 70–74.
[32] N. Calvar, I. Domínguez, E. Gómez, Á. Domínguez, Separation of binary mixtures aromatic+aliphatic using ionic liquids: influence of the structure of the ionic liquid, aromatic and aliphatic, Chem. Eng. J. 175 (2011) 213–221.
[33] S. García, J. García, M. Larriba, J.S. Torrecilla, F. Rodríguez, Sulfonate-based ionic liquids in the liquid–liquid extraction of aromatic hydrocarbons, J. Chem. Eng. Data. 56 (7) (2011) 3188–3193.
[34] H. Kuramochi, K. Maeda, S. Kato, M. Osako, K. Nakamura, S.-I. Sakai, Application of UNIFAC models for prediction of vapor–liquid and liquid–liquid equilibria relevant to separation and purification processes of crude biodiesel fuel, Fuel. 88 (8) (2009) 1472–1477.
[35] J. Kang, D. Gu, T. Wu, M. Wang, H. Zhang, H. Guo, Y. Yin, Y.i. Yang, J. Tian, An approach based upon the consecutive separation and the economical two-phase solvent system preparation using UNIFAC mathematical model for increasing the yield of high-speed counter-current chromatography, Sep. Purif. Technol. 162 (2016) 142–147.
[36] X.u. Zhao, Q. Yang, D. Xu, Z. Bao, Y.i. Zhang, B. Su, Q. Ren, H. Xing, Design and screening of ionic liquids for C_2H_2/C_2H_4 separation by COSMO-RS and experiments, AIChE J. 61 (6) (2015) 2016–2027.
[37] M. Gonzalez-Miquel, M. Massel, A. DeSilva, J. Palomar, F. Rodriguez, J. F. Brennecke, Excess enthalpy of monoethanolamine + ionic liquid mixtures: how good are COSMO-RS predictions, J. Phys. Chem. B. 118 (39) (2014) 11512–11522.
[38] X. Pu, L. Wu, Y. Liu, Prediction of vapor-liquid equilibrium properties for the mixture of propylene+propane from the combined use of Peng-Robinson equation of state and COSMO-RS model, Int. J. Chem. Eng. Appl. 8 (2) (2017) 92–96, https://doi.org/10.18178/ijcea.2017.8.2.636.
[39] Y. Cao, Z. Wu, Y. Zhang, Y. Liu, H. Wang, Screening of alternative solvent ionic liquids for artemisinin: COSMO-RS prediction and experimental verification, J. Mol. Liq. 338 (2021) 116778, https://doi.org/10.1016/j.molliq.2021.116778.

[40] M. Fallanza, M. González-Miquel, E. Ruiz, A. Ortiz, D. Gorri, J. Palomar, I. Ortiz, Screening of RTILs for propane/propylene separation using COSMO-RS methodology, Chem. Eng. J. 220 (2013) 284–293.
[41] G. Gonfa, M.A. Bustam, A.M. Sharif, N. Mohamad, S. Ullah, Tuning ionic liquids for natural gas dehydration using COSMO-RS methodology, J. Nat. Gas Sci. Eng. 27 (2015) 1141–1148.
[42] Y. Chen, Computer-aided design methodology for separation processes with ionic liquids, DTU, 2020. PhD dissertation,.
[43] A. Arce, M.J. Earle, H. Rodríguez, et al., Separation of benzene and hexane by solvent extraction with 1-alkyl-3-methylimidazolium bis (trifluoromethyl) sulfonyl amide ionic liquids: effect of the alkyl-substituent length, J. Phys. Chem. B. 111 (18) (2007) 4732–4736, https://doi.org/10.1021/jp066377u.
[44] P.F. Requejo, N. Calvar, Á. Domínguez, E. Gómez, Comparative study of the LLE of the quaternary and ternary systems involving benzene, n-octane, n-decane and the ionic liquid [BMpyr][NTf_2], J. Chem. Thermodyn. 98 (2016) 56–61.
[45] E. Gómez, I. Domínguez, N. Calvar, J. Palomar, Á. Domínguez, Experimental data, correlation and prediction of the extraction of benzene from cyclic hydrocarbons using [Epy][ESO_4] ionic liquid, Fluid Phase Equilibr. 361 (2014) 83–92.
[46] B. Mokhtarani, J. Musavi, M. Parvini, et al., Experimental study on liquid–liquid equilibria of ionic liquids+ alkane+ ethyl benzene or p-xylene at 298.15 K, Fluid Phase Equilibr. 409 (2016) 7–11, https://doi.org/10.1016/j.fluid.2015.08.031.
[47] Y. Dong, Q. Yang, Z. Li, Z. Lei, Extractive distillation of the benzene and acetonitrile mixture using an ionic liquid as the entrainer, Green Energy Environ. 6 (3) (2021) 444–451.
[48] Y. Guo, F. Shi, Q. Shu, X. Yue, C. Wang, L. Tao, J. Li, Liquid-liquid equilibrium for n-hexane+ benzene+ sulfolane,+ 1-ethyl-3-methylimidazolium bis (trifluoromethylsulfonyl) imide ([EMIM][NTf_2]),+ 1-ethyl-3-methylimidazolium ethylsulfate ([EMIM][$EtSO_4$]) and+ the mixtures of [EMIM][NTf_2] and [EMIM][$EtSO_4$], Fluid Phase Equilibr. 529 (2021) 112882, https://doi.org/10.1016/j.fluid.2020.112882.
[49] P. Navarro, M. Larriba, N. Delgado-Mellado, M. Ayuso, M. Romero, J. García, F. Rodríguez, Experimental screening towards developing ionic liquid-based extractive distillation in the dearomatization of refinery streams, Sep. Purif. Technol. 201 (2018) 268–275.
[50] M. Larriba, P. Navarro, J. García, F. Rodríguez, Liquid–liquid extraction of toluene from heptane using [emim][DCA], [bmim][DCA], and [emim][TCM] ionic liquids, Ind. Eng. Chem. Res. 52 (7) (2013) 2714–2720.
[51] M. Larriba, P. Navarro, J. García, F. Rodríguez, Liquid–liquid extraction of BTEX from reformer gasoline using binary mixtures of [4empy][Tf2N] and [emim][DCA] ionic liquids, Energ. Fuel. 28 (10) (2014) 6666–6676.
[52] P. Navarro, M. Ayuso, A.M. Palma, M. Larriba, N. Delgado-Mellado, J. García, F. Rodríguez, J.A.P. Coutinho, P.J. Carvalho, Toluene/n-heptane separation by extractive distillation with tricyanomethanide-based ionic liquids: experimental and CPA EoS modeling, Ind. Eng. Chem. Res. 57 (42) (2018) 14242–14253.
[53] M. Ayuso, P. Navarro, A.M. Palma, M. Larriba, N. Delgado-Mellado, J. García, F. Rodríguez, J.A.P. Coutinho, P.J. Carvalho, Toward modeling the aromatic/aliphatic separation by extractive distillation with tricyanomethanide-based ionic liquids using CPA EoS, Ind. Eng. Chem. Res. 58 (42) (2019) 19681–19692.
[54] M. Ayuso, A.M. Palma, M. Larriba, N. Delgado-Mellado, J. García, F. Rodríguez, J. A.P. Coutinho, P.J. Carvalho, P. Navarro, Experimental and CPA EoS description of the key components in the BTX separation from gasolines by extractive distillation with tricyanomethanide-based ionic liquids, Ind. Eng. Chem. Res. 59 (33) (2020) 15058–15068.
[55] J.A. Lazzús, A group contribution method to predict the melting point of ionic liquids, Fluid Phase Equilibr. 313 (2012) 1–6, https://doi.org/10.1016/j.fluid.2011.09.018.
[56] Y. Chen, G.M. Kontogeorgis, J.M. Woodley, Group contribution based estimation method for properties of ionic liquids, Ind. Eng. Chem. Res. 58 (10) (2019) 4277–4292, https://doi.org/10.1021/acs.iecr.8b05040.
[57] Y. Chen, X. Liu, J.M. Woodley, G.M. Kontogeorgis, Gas solubility in ionic liquids: UNIFAC-IL model extension, Ind. Eng. Chem. Res. 59 (38) (2020) 16805–16821.
[58] B.C. Roughton, B. Christian, J. White, K.V. Camarda, R. Gani, Simultaneous design of ionic liquid entrainers and energy efficient azeotropic separation processes, Comput. Chem. Eng. 42 (2012) 248–262.
[59] Y. Lei, Z. Yu, Z. Wei, X. Liu, H. Luo, Y. Chen, X. Liang, G.M. Kontogeorgis, Energy-efficient separation of propylene/propane by introducing a tailor-made ionic liquid solvent, Fuel. 326 (2022) 124930, https://doi.org/10.1016/j.fuel.2022.124930.
[60] D. Karlovic, M. Sovilj, J. Turkulov, Kinetics of oil extraction from corn germ, J. Am. Oil Chem. Soc. 69 (5) (1992) 471–476, https://doi.org/10.1007/BF02540952.
[61] Q. Li, N. Hu, S. Zhang, Q. Wu, J. Qi, Energy-saving heat integrated extraction-azeotropic distillation for separating isobutanol-ethanol-water, Sep. Purif. Technol. 255 (2021) 117695, https://doi.org/10.1016/j.seppur.2020.117695.
[62] N. Saxena, N. Mali, S. Satpute, Study of thermally coupled distillation systems for energy-efficient distillation, Sadhana ACAD, P. Eng. S. 42 (1) (2017) 119–128, https://doi.org/10.1007/s12046-016-0580-x.
[63] S. Righi, A. Morfino, P. Galletti, C. Samorì, A. Tugnoli, C. Stramigioli, Comparative cradle-to-gate life cycle assessments of cellulose dissolution with 1-butyl-3-methylimidazolium chloride and N-methyl-morpholine-N-oxide, Green Chem. 13 (2) (2011) 367–375.
[64] Y. Huang, X. Zhang, X. Zhang, H. Dong, S. Zhang, Thermodynamic modeling and assessment of ionic liquid-based CO_2 capture processes, Ind. Eng. Chem. Res. 53 (29) (2014) 11805–11817.